Characterisation of Compressed Windings via High Resolution X-ray Computed Tomography and Semi-Automatic Segmentation

Joshua Hoole
Electrical Energy Management Group
University of Bristol
Bristol, United Kingdom
josh.hoole@bristol.ac.uk

Ria L. Mitchell
Department of Materials Science and Engineering
University of Sheffield
Sheffield, United Kingdom
r.mitchell@sheffield.ac.uk

Dominic North
Electrical Energy Management Group
University of Bristol
Bristol, United Kingdom
dj.north@bristol.ac.uk

Nick Simpson
Electrical Energy Management Group
University of Bristol
Bristol, United Kingdom
nick.simpson@bristol.ac.uk

Philip H. Mellor
Electrical Energy Management Group
University of Bristol
Bristol, United Kingdom
p.h.mellor@bristol.ac.uk

***Abstract*—Compressed windings can substantively increase the power density of electrical machines. However, the compression of coils can lead to significant deformation of the conductor lay, cross-sections and insulation coating, impacting the longevity, loss and thermal performance of such windings. This paper presents the use of high resolution X-ray Computed Tomography (XCT), along with 2D and 3D image segmentation techniques, to perform an initial characterisation of a compressed aluminium winding. From the XCT derived data, significant localised conductor deformation and strand insulation thinning has been observed.**

***Index Terms*—computed tomography, compressed windings**

I. Introduction

The ever-increasing adoption of electrical machines in automotive and aerospace sectors is leading to the need for a significant increase in machine power density [1]. One route to lightweight electrical machines is the use of compressed aluminium stator windings, which lead to high fill factors with a lower mass compared to equivalent copper windings [2].

Power dense electrical machines often adopt AC excitation frequencies in excess of 1 kHz and multi-strand stator windings are required to mitigate the resulting skin effect losses [3]. However, such windings are susceptible to proximity and bundle-level losses [3]. As a result, the compressed winding shown in Fig. 1 consists of 10 turns of 8 parallel 'strands-in-hand' of 1.4 mm diameter. The strands are transposed by twisting prior to compression with the aim of achieving a uniform strand arrangement similar to a Litz-type winding. AC losses are highly sensitive to the achieved conductor lay in the stator slot [1], [2]. The mechanical compaction of the windings can lead to significant deformation of both the conductor and strand insulation, potentially leading to the failure of the coil, which has been the focus of prior studies in the literature [2].

This work was funded by the EPSRC Impact Acceleration Account Net Zero Fund. The authors acknowledge the University of Sheffield Tomography Centre (STC) funding from EPSRC (EP/T006390/1).

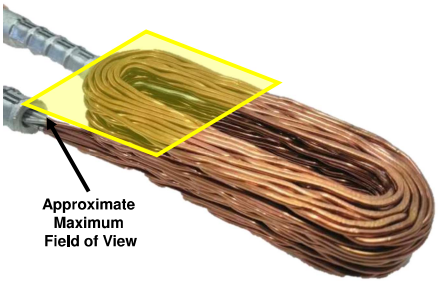

Fig. 1. The compressed aluminium multi-stranded coil

Previous work has identified the typical conductor cross-sections in compressed windings via Finite Element Analysis (FEA) simulation [4] and the sectioning of manufactured coils [1]. To date, the characterisation of the conductor lay and cross-sections in as-manufactured windings has been focused on establishing the thermal performance of the compressed winding [4]–[6]. Previous work has also considered the AC losses of compressed windings with a focus on the impact of strand transposition within manufactured coils [1], [7].

This paper will explore the novel use of high resolution X-ray Computed Tomography (XCT) and image processing methods to characterise the conductor lay and insulation thinning of a compressed aluminium winding. In addition, a methodology to generate 2D and 3D FEA models for AC loss estimation of compressed windings will also be presented, stepping towards the realisation of high-fidelity Digital Twins.

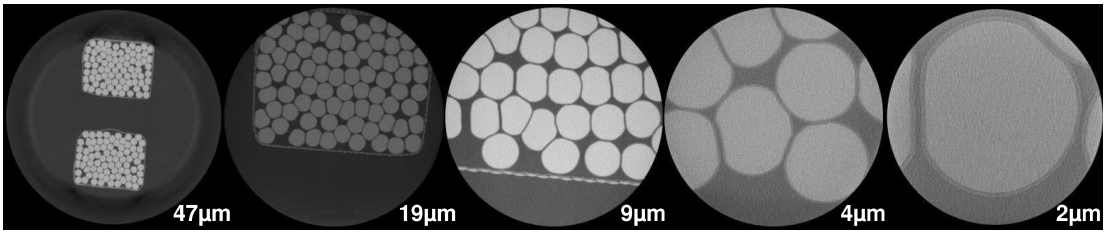

Fig. 2. Examples of XCT slices within the winding active length for decreasing fields of view and increasing resolution

TABLE I
XCT SCANNING PARAMETERS

Voxel Size (μm)	Tube Voltage (kV)	Tube Current (μA)	Source Power (W)	Magnification	Exposure Time (s)	Scan Time (Hr)
47.29	100	140	14	0.4x	1	1.0
18.84	150	154	23	0.4x	1	1.0
8.86	160	156	25	0.4x	4	2.5
3.98	160	156	25	4.0x	4	2.5
1.94	160	156	25	4.0x	18	9.0

II. HIGH RESOLUTION X-RAY COMPUTED TOMOGRAPHY

XCT provides a non-destructive approach to generating information on the internal structures of objects by reconstructing a 3D model from a large number of 2D X-ray projections [8]. A significant advantage of XCT approaches for electrical machine windings is that XCT will not disturb the conductor lay, which might occur when physically sectioning coil samples [8]. XCT has previously been used to characterise electrical machine insulation materials [9], [10] and for assessing varnish impregnation of coils [11]. The winding shown in Fig. 1 was scanned using a Zeiss Xradia Versa 620 X-ray Microscope (XRM). Due to the available field of view of the XRM, only half of the winding was scanned (see Fig. 1).

The 'Scout and Zoom' functionality of the XRM was used to generate higher-resolution scans of the winding in decreasing voxel (the 3D equivalent of a pixel) sizes across 47μm, 19μm, 9μm, 4μm and 2μm as shown in Fig. 2. Scanning parameters are shown in Table I and a HE4 filter was used for all scans with 1,601 X-ray projections being taken.

Fig. 2 shows the 'slices' at a various locations in the winding active length, generated from the XCT scan and highlights the functionality of the 'scout and zoom' function, where the Field of View (FoV) is decreased from: encapsulating the entire winding cross-section (including end winding); the majority of a single slot; to clusters of conductors with the insulation around each aluminium strand. Across the XCT slices, the impact of compression during manufacture can be clearly observed, with the original circular conductor cross-sections being deformed, including changes in cross-sectional area.

A. Characterization of Conductor Cross-Sections

In order to quantify the deformation of the conductor cross-sections shown previously in Fig. 2, image segmentation techniques were employed to identify the area and circularity 'k' as computed using (1), where A and P are the cross-sectional area and perimeter respectively. For a perfect circle, $k = 1$ and any deviation from a circle results in $k < 1$. The simulation studies performed previously by Kulan et al. yielded approximate values of $k = 0.85$ to 0.97 for compressed windings [4]. In contradiction to this previous work, it can be observed from Fig. 3 that in this instance, the conductor lay does not conform to a regular arrangement, with various conductors demonstrating different levels of deformation and positioning within the stator slot and end winding.

$$k = \frac{4\pi A}{P^2} \tag{1}$$

Image segmentation concerns the development of semi- and fully-automatic processes to extract objects of interest from images [13]. Image segmentation of winding XCT slices is challenging due to windings consisting of a large number of objects with near-identical density and hence greyscale intensity within an image. In addition, at lower resolutions (>20μm voxel size), the authors have observed 'bleed' in greyscale intensity between conductors, complicating image segmentation of non-regular shapes. Consequently, the partial slot FoV at 18μm was required to apply automated segmentation. Automatic processes are vital due to the large number of conductors per slot (80) and the large number of XCT slices (700) that comprise of the active FoV length at 18μm.

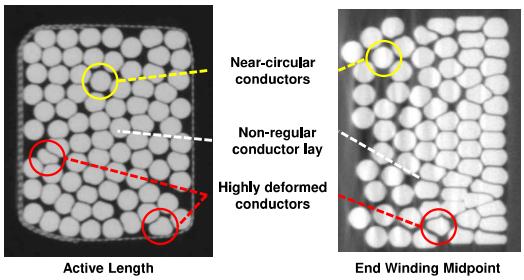

Fig. 3. Demonstration of conductor lay and cross-section deformation

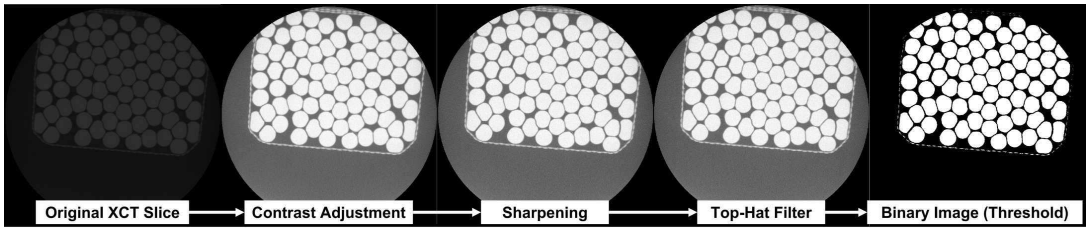

Fig. 4. The filtering and image segmentation process adopted to characterise conductor cross-sections

Image filters were applied to each XCT slice, as shown in Fig. 4: contrast enhancement; unsharp masking (to sharpen the image); and a top-hat filter (which enhances the difference between objects and the background) [13]. The image was segmented by setting a greyscale intensity threshold, where if a pixel has an intensity $>$ 50,000 (white = 65,535), it belongs to a conductor. The area and k of each complete conductor within the binary 18μm FoV could then be computed, by identifying the number of pixels and the perimeter of each contiguous region. Image processing was conducted in MATLAB®.

From processing the 700 XCT slices, approximately 50,000 individual complete conductor cross-sections were identified. Fig. 5 shows the variability in the resulting conductor cross-sectional area, with reference to a value of 1.54mm^2 for the original circular conductors. Fig. 5a highlights that the compression of the strands leads to both reduced and increased conductor cross-sectional areas, suggesting that there is also significant deformation along the strand length to accommodate the area changes. The median conductor cross-sectional area was found to approximate the original area at 1.54mm^2.

The conductor k variability is shown in Fig. 5b. It can be observed that all conductors have deformed from a perfect circle and the insets to Fig. 5b show the cross-sections leading to minimum k values. It was also observed that the minimum k values occurred for conductors that also had the greatest cross-sectional area deviation. When coupled with the long distribution tails in Figs. 5a and 5b, it can be concluded that during compression, deformation does not occur uniformly across all conductors and is localised to individual conductors, which may lead to strands severing during manufacture. Finally, Figs. 5c and 5d show the locations of the minimum (defined as the 10th percentile) area and k values, where it can be observed that minimum areas typically occur around the coil edges (Fig. 5c), whilst minimum k values are clustered together (Fig. 5d).

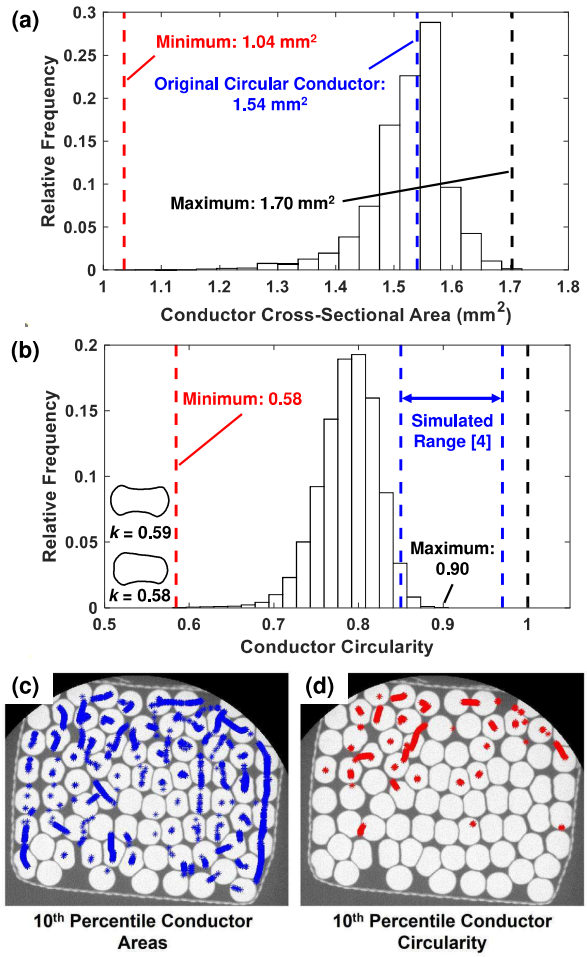

Fig. 5. Variability in conductor a) cross-sectional area and b) circularity along with the typical positions of minimum values in c) and d) respectively

B. Construction of Dedicated Finite Element Analysis Models

The AC losses of multi-strand windings can be estimated using 2D electromagnetic Finite Element Analysis (FEA) [3]. In order to support the investigation into the impact of compression on the AC losses of the winding within future work, the conductor lays and shapes identified within the XCT scan could be used to form dedicated geometries in an FEA environment that is fully scriptable [12], as shown in Fig. 6.

However, as the 18μm FoV did not contain all of the conductors within a stator slot, the lower resolution 47μm XCT slices were required. As the 47μm XCT slices contained greyscale intensity 'bleed' between conductors, the previous process could not reliably differentiate between individual conductors. Therefore, the greyscale threshold for segmentation had to be increased in increments to separate conductors. As such a method led to smaller conductor areas than present in the actual sample, the conductor areas were re-scaled about their individual centroid to achieve the areas present in the corresponding XCT slice at the 18μm resolution. The stepped

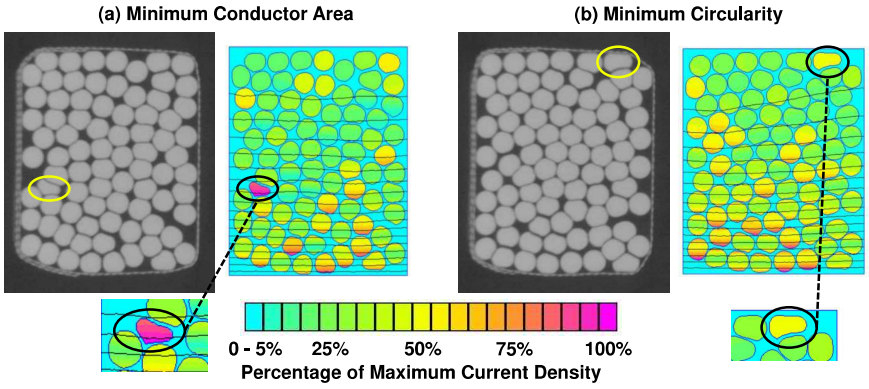

Fig. 6. Current density in conductors with minimum a) cross-sectional area and b) circularity as computed using 2D FEA at 1.2kHz AC excitation

edges of the extracted conductor shapes were then smoothed using a 3rd-order Savitzky-Golay filter [14].

The two XCT slices with the minimum k and area values were converted into the 2D FEA environment (see Fig. 6). A random strand-in-hand assignment was assumed as the strand arrangement is currently unknown due to only performing a half-coil scan. The AC losses were evaluated at an AC frequency of 1.2 kHz. The assumed end winding inductance was tuned such that the predicted AC loss magnitudes were similar to those observed from impedance analyzer testing [7] of coils from the production batch. Fig. 6 shows that the current density in both the minimum area and k conductors are higher than other conductors at a similar slot position. High current densities in individual conductors will lead to localised heating, potentially leading to insulation failure, which may be compounded by insulation thinning. Whilst the increased current densities may be exacerbated by the assumed strand arrangement, further investigation into the link between AC losses and conductor compression is warranted.

C. Characterization of Insulation Thinning

An initial investigation into the insulation thickness within the compressed winding was also performed using XCT. The conductor insulation was found to be visible across the 9μm, 4μm and 2μm FoVs as shown in Fig. 7. However, there was significant noise within the 4μm and 2μm FoVs and therefore, the 9μm FoV was selected. To support conductor insulation segmentation, the contrast of the XCT slice was enhanced and a median filter applied to reduce noise in the image as shown in Fig. 7 [13]. It was found that in the greyscale image the conductor insulation presented intensity values of between 35,000 and 50,000, with these values being used to segment the insulation layers as shown in Fig. 8.

Fig. 8 shows a round conductor, which provided a baseline insulation thickness of 53.2μm (6 pixels), in agreement with manufacturer's datasheets. Fig. 8 also shows a highly deformed conductor, with an estimated insulation thickness of 17.1μm (2 pixels), a 68% reduction indicating that significant thinning of insulation can occur during the manufacture of compressed windings, potentially leading to inter-turn shorts [2].

Future work will automate the insulation thickness estimation such that it could be applied to multiple conductors and slices, to generate statistically significant insulation thickness variability histograms in a similar manner to those in Fig. 5, using noise filtering to exploit the 4μm and 2μm FoV.

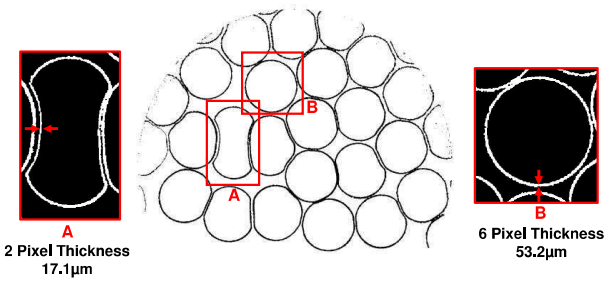

Fig. 8. Strand insulation thickness estimation from segmented image

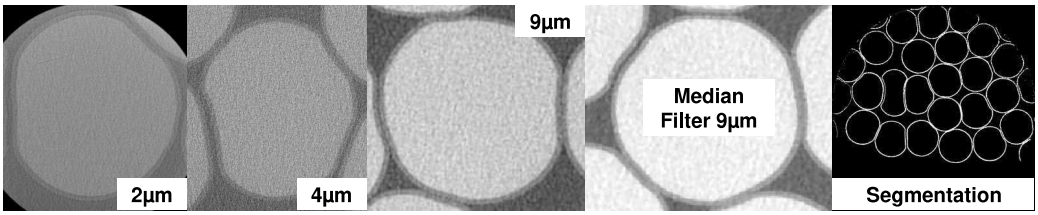

Fig. 7. Visualisation of conductor insulation at various resolutions and segmentation process adopted to identify insulation

III. Tracing of Strand Paths via Semi-Automatic Volume Segmentation

In previous work, it was identified that tracing strand paths around end windings of a distributed, random wound machine required a time-consuming and manual approach [8]. In addition, such an approach only provided a guide of the strand path, rather than a 3D geometry of an individual strand. As the XCT scanning performed in Section II provided a higher resolution scan of an end winding, albeit a compressed and concentrated winding, a semi-automatic approach to segmenting the 3D geometry of individual strands was investigated.

In addition to the filters described in Section II-A, a Watershed Segmentation (WS) transform was applied to the 3D stack of XCT slices. WS automatically segments objects within 3D volumes using the voxel greyscale intensity to define 'ridgelines' that separate areas of high or low intensity [13]. However, WS leads to 'over-segmentation' where individual conductors are further segmented (i.e. the shapes shown in Fig. 4 are divided further across conductor faces).

Whilst over-segmentation meant that WS was not appropriate for the conductor segmentation performed in Section II-A, WS can still be of use to generate the 3D geometry of individual strands. The WS approach produces many sub-volumes within the original XCT volume. Therefore, an algorithm was developed to assist the user in searching through the volume space to trace the paths of individual strands and ultimately reconstruct the 3D geometry of individual strands.

Firstly, each sub-volume consists of all the voxels generated from the WS. From this, the outer surface of the sub-volume can be derived. The centroid of the volume can also be computed. It is proposed that the centroid can be used to find the next sub-volume of a given strand, as the next volume should lie close to the path direction previously taken by the strand (described by a 3D search vector). As a result, the closet sub-volume that is penetrated by the 3D search vector is highlighted as the most probable next sub-volume. This process is visualised in Fig. 9, where green volumes are the previous strand, the red volume is the current sub-volume and the yellow volume is the proposed next sub-volume. To minimise computational expense, only 50 of the nearest sub-volumes are considered and a convex-hull representation of the sub-volume is used. The algorithm is repeated until the strand path is complete. At this stage, the convex-hull representations are returned to the actual sub-volume voxels and surface.

The WS over-segmentation can lead to irregular shapes and centroid positions, preventing a fully-automatic process. The user is therefore required to accept the suggested sub-volume, or propose the next sub-volume using its identification number. This semi-automatic process was performed for all 80 strands, resulting in the example 3D geometries shown in Fig. 10 and the transposition of the strands can be clearly shown. The tracing of individual strands is also visualised in Fig 11. Scanning of the full coil in future work would permit the strand assignment throughout the winding to be defined. Within the segmentation, it was observed that one of the strands had completely fractured during compression, as shown in Fig. 10 and confirmed by electrical continuity measurement [2].

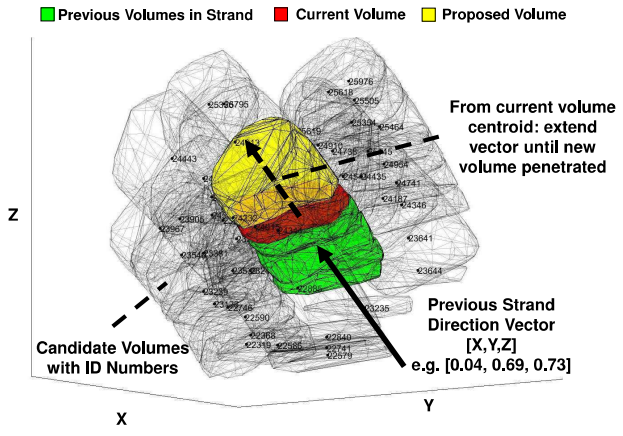

Fig. 9. Semi-automatic 3D volumetric strand tracing process

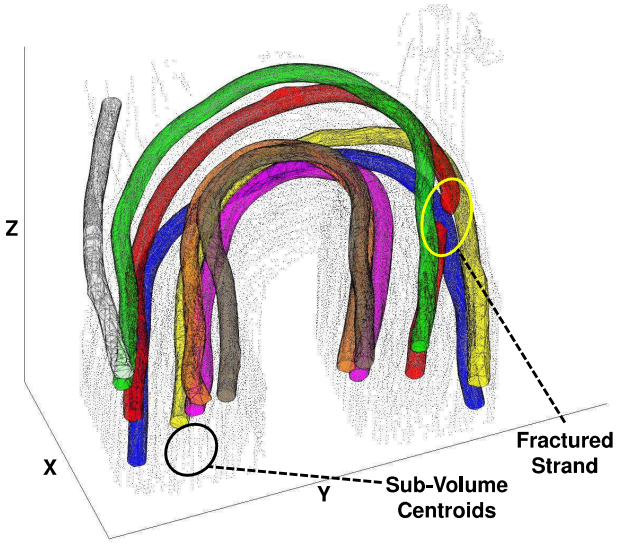

Fig. 10. 3D visualisation of select segmented strand geometries, including a fractured strand and tail terminations strand

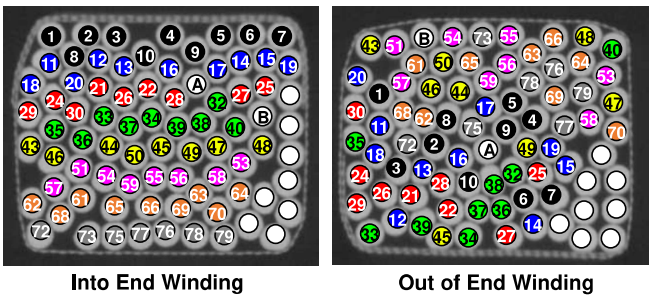

Fig. 11. Demonstration of strand transposition through the end winding, where numeric values show complete strands, lettered positions highlight fractured strands and blank positions represent tail strands running to the termination connectors

The average time to perform the segmentation for a single strand was 9 minutes and is expected to be faster than the time required to manually segment a strand on slice-by-slice basis. The algorithm identified the correct next volume in 94% of cases highlighting that it could be the basis for a fully-automatic approach with further development and refinement.

IV. Discussion

The presented techniques have shown the utility of high resolution XCT for characterising compressed winding conductor lay and cross-sections. XCT scans could provide data to support future modelling campaigns across thermal, voltage stress, AC loss and manufacturing fault investigations. It is not proposed that every manufactured coil is inspected via XCT for insulation integrity checks or quality control as lower-cost options exist [2], [15]. However, XCT of compressed coils provides a route to linking manufacturing process parameters (e.g. compression force, rate and hold time [4]) to the conductor lay and cross-sections and the coil thermal and loss characteristics. For example, the coil scanned within this work showed localised conductor deformation, including strand fracture and was likely over-compressed during manufacture, compared to the regular lays presented by Kulan et al. [4].

Consequently, XCT could be used to firstly validate compression simulations and identify the manufacturing parameters that minimise undesirable conductor deformation, or to compare different slot compression techniques such as those described by Sell-Le Blanc et al. [16]. In addition, XCT also has the potential to quantify the levels of insulation thinning that occur during the manufacture of compressed windings.

Regarding the AC losses of compressed coils, Widmer et al. highlight the importance of achieving uniform strand transposition [1]. In future work, the 3D strand paths identified in Section III could be used to verify that the strand twisting performed has achieved the desired Litz-type strand transposition. In addition, an XCT scan of the entire coil could support the development of a 3D electromagnetic FEA model, by forming a mesh based on the assembled sub-volumes for each strand. Such a model would contribute towards investigating the 3D AC loss effects within as-manufactured compressed coils and, when coupled with a complementary thermal model, could enable assessment of localised strand heating, not possible via invasive experimental measurement.

V. Conclusion

The push towards power-dense electrical machines has encouraged the development of compressed windings. However, the compression manufacturing process employed can lead to highly deformed conductor lays and cross-sections, along with strand insulation thinning. This paper presented the application of high resolution X-ray Computed Tomography (XCT) and image segmentation techniques to identify the conductor characteristics in a manufactured compressed aluminium coil.

Performing XCT at various resolutions identified that localised deformation of conductors can occur within compressed windings, potentially leading to increased losses and heating of individual strands within the winding. In addition, high resolution XCT was able to quantify the levels of insulation thinning resulting from compression of the coil.

Within future work, the semi-automatic image segmentation techniques employed could be adopted to identify how manufacturing process parameters impact the thermal performance and AC loss of compressed windings via the construction of dedicated 2D and 3D Finite Element Analysis models.

Acknowledgment

This work was funded by the EPSRC Impact Acceleration Account Net Zero Fund. The authors acknowledge the University of Sheffield Tomography Centre (STC) funding from EPSRC (EP/T006390/1).

References

[1] J. D. Widmer, R. Martin, and B. C. Mecrow, "Precompressed and Stranded Aluminum Motor Windings for Traction Motors," IEEE Trans. Ind. Appl., vol. 52, no. 3, pp. 2215–2223, 2016.

[2] D. North, J. Hoole, N. Simpson, and P. Mellor, "Test Metrics and Damage Fingerprints in Multistranded Compressed Aluminium Windings," 2021 IEEE Energy Conversion Congress and Exposition (ECCE), pp. 3789–3796, 2021.

[3] P. Mellor, J. Hoole, and N. Simpson, "Computationally efficient prediction of statistical variance in the AC losses of multi-stranded windings," 2021 IEEE Energy Conversion Congress and Exposition (ECCE), pp. 3887–3894, 2021.

[4] M. C. Kulan, N. J. Baker, and J. D. Widmer, "Design and Analysis of Compressed Windings for a Permanent Magnet Integrated Stater Generator," IEEE Trans. Ind. Appl., vol. 53, no. 4, pp. 3371–3378, 2017.

[5] S. Ayat, H. Liu, M. Kulan, and R. Wrobel, "Estimation of Equivalent Thermal Conductivity for Electrical Windings with High Conductor Fill Factor," 2018 IEEE Energy Conversion Congress and Exposition (ECCE), pp. 6529–6536, 2018.

[6] M. Halwas, F. Hoffmann, P. Bader, T. Heyde, M. Doppelbauer, and J. Fleischer, "Influence of Wire Layer Structures on the Thermal Behavior in Electrical Machine Slots," 2021 11th International Electric Drives Production Conference (EDPC), 2021.

[7] R. Wrobel, N. Simpson, P. H. Mellor, J. Goss, and D. A. Staton, "Design of a Brushless PM Starter Generator for Low-Cost Manufacture and a High-Aspect-Ratio Mechanical Space Envelope," IEEE Trans. Ind. Appl., vol. 53, no. 2, pp. 1038–1048, 2017.

[8] J. Hoole, N. Simpson, P. H. Mellor, and A. Daanoune, "Experimental Determination of Conductor Lay and Impact on AC Loss in Volume Manufactured Machines using X-Ray Computed Tomography," 2021 IEEE Energy Conversion Congress and Exposition (ECCE), pp. 3873–3880, 2021.

[9] A. Contin, M. Piller, and G. Schena, "Analysis of 3D Computed Tomographic Imaging of Ground-wall Insulation for AC rotating machines," IEEE Trans. Dielectr. Electr. Insul., vol. 22, no. 3, pp. 1520–1529, 2015.

[10] C. Sáxen, E. Kristofer Gamstedt, R. Afshar, G. Paulsson, and F. Sahlén, "A Micro-Computed Tomography Investigation of the Breakdown Paths in Mica/Epoxy Machine Insulation," IEEE Trans. Dielectr. Electr. Insul., vol. 25, no. 4, pp. 1553–1559, 2018.

[11] Y. Guo, J. Soulard, and D. Greenwood, "Challenges in Electric Machine Stator Manufacturing and Their Influences on Thermal Performance," 2019 9th International Electric Drives Production Conference (EDPC), 2019.

[12] D. Meeker, Finite Element Method Magnetics (FEMM), Version 4.2.

[13] R. Gonzalez, and R. Woods, Digital Image Processing, 4th Ed., Pearson Education Ltd., 2017.

[14] R. W. Schafer, "What is a Savitzky-Golay Filter? [Lecture Notes]," IEEE Signal Process. Mag., vol. 28, no. 4, pp. 111–117, 2011.

[15] M. C. Kulan, and N. J. Baker, "Life-time characteristics of random wound compressed stator windings under thermal stress," IET Electr. Power Appl., vol. 13, no. 9, pp. 1287–1297, 2019.

[16] F. Sell-Le Blanc et al."Feasibility Study for Enameled Round Copper Wire Compression within Slots of Electrical Machines," 9th International Electric Drives Production Conference (EDPC), 2019.